Wave Velocities and Poisson Ratio in a Loose Sandy Martian Regolith Simulant Under Low Stresses: 2. Theoretical Analysis

Bernardo Caicedo, Juan-Pablo Castillo Betancourt, Pierre Delage, Philippe Lognonné, William Bruce Banerdt

WAVE VELOCITIES AND POISSON RATIO IN A LOOSE SANDY MARTIAN REGOLITH SIMULANT
PART 2: THEORETICAL ANALYSIS

B. Caicedo[1], J. P. Castillo Betancourt[1,2], P. Delage[2], Ph. Lognonné[3], B. Banerdt[4]

[1] Universidad de los Andes, Bogota, Colombia.

[2] Ecole des Ponts ParisTech, lab. Navier-CERMES, CNRS, UGE, Marne la Vallée, France.

[3]Université Paris-Cité, Institut de Physique du Globe, CNRS, Paris, France.

[4] Jet Propulsion Laboratory, California Institute of Technology, Pasadena, California, USA.

Corresponding author: Bernardo Caicedo (bcaicedo@uniandes.edu.co)

Journal of Geophysical Research: Planets, 10.1029/2023JE008008

Key points:

- A novel theory based on contact mechanics was proposed to calculate V_p and V_s of uniform granular materials.
- The theory considers the roughness of the particles, the stress, the porosity of the granular assembly and the properties of the grains.
- Theoretical results agree with experimental measurements on loose samples of Fontainebleau sand used as a Mars regolith simulant.

ABSTRACT

This paper presents a theoretical analysis of the data on wave velocities measurements at small stresses presented in a companion paper (Castillo-Betancourt et al. 2023) on a Martian regolith loose sandy simulant (Fontainebleau sand) of the soil at the InSight landing site on Mars (Elyseum Planitia). Experimental data of wave velocities and Poisson's ratio are interpreted in the light of a granular contact mechanics theory (Bachrach et al. 2000) and completed accounting for rugosity effects (Bahrami et al. 2005, Butt et al. 2015), that are suspected to have stronger effects in sands under low stresses. The asperities of a grain of Fontainebleau sand were investigated through Atomic Force Microscopy, but larger asperities had to be adopted so as to better fit the model prediction with experimental data. A good agreement between the experimental data and the model predictions is obtained for stress above 10 kPa. Below 5 kPa, an area in which asperities are suspected to have a stronger influence, the model is not fully satisfactory, showing that further experimental and theoretical investigation are necessary in a stress zone particularly relevant to surface soils in planets, with probably enhanced effects of asperities on the intergrains contact mechanics.

PLAIN LANGUAGE SUMMARY

To better understand seismic wave propagation at the surface of the InSight landing site on Mars, this paper presents a theoretical interpretation of the seismic wave velocities at low stress measured in a sand sample used as Martian regolith simulant, presented in a companion paper. The theory is based on both a theoretical elastic model of a pack of smooth spheres of same diameter and an approach accounting for the effects of local rugosity at the contact between sand grains (rugosity is supposed to have a stronger influence at the low stresses resulting from the smaller gravity on Mars). The sphere pack model shows that some slippage between grains is necessary to properly account for the radial deformation of a cylindrical sample submitted to an increase in axial stress (as described by an elastic parameter called the Poisson ratio). Accounting for rugosity effects allows a better prediction of the changes in wave velocity with respect to stress. The decrease in velocity under decreased stress is confirmed, but the rugosity parameter measured by using an Atomic Force Microscope was under-estimated, probably due to the over-simplistic hypothesis of considering spheres. Proper prediction was obtained by fitting this parameter at a twice larger value.

NOTATION

a	Radius of the contact area between spherical particles
A_H	Contact area between spherical particles, $A_H = \pi a^2$
a	Hertzian radius of the contact area between spherical particles.
a_R	Radius of the contact area between rough spherical particles.
a'_R	Non-dimensional contact radius
$a_1..a_9$	Constants of the gamma function.
B(0.5,γ+1)	Beta function.
D_{50}	Median particle size.
E	Young Modulus.
E'	Effective Young modulus $1/E' = (1-\nu^2)/E$
F	Particle contact force.
G	Shear Modulus.
G_{HM}	Shear modulus from the Hertz-Mindlin model.
H_{mic}	Asperities microhardness
K_{HM}	Bulk modulus from the Hertz-Mindlin model.
n	Coordination number.
P_0	Pressure on the contact between particles.
$P(r)$	Pressures at all microcontacts on rough spherical particles.
P'_0	Non-dimensional pressure distribution
R_g	Particle radius.
R_c	Curvature radius at the contact between particles.
S_n	Normal contact stiffness.
S_n^{HM}	Normal contact stiffness for perfect smooth particles.
S_n^{Rough}	Normal contact stiffness for rough particles.
S_t	Tangential contact stiffness.
S_t^{mix}	Tangential stiffness for a mixture of slipping and non-slipping particles.
V_p	Compression wave velocity.
Vs	Shear wave velocity.

α Non-dimensional parameter for characterising the particle's roughness.

δ_H Maximum displacement for a Hertz Mindlin contact between spherical particles.

δ_R Maximum displacement between rough spherical particles.

ϕ Sample porosity.

ν Poisson Ratio

ν_g Poisson Ratio of the particles.

ν_{HM} Poisson Ratio given by the Herz-Mindlin theory.

σ_3 Mean stress.

σ_{rms} RMS asperities height.

τ Non-dimensional parameter for characterising the particle's roughness.

ξ Proportion of non-slipping particles.

Keywords

Wave velocities, Martian regolith, Hertz Mindlin, Contact theory, InSight mission.

1. INTRODUCTION

The elastic behaviour of sands under low stresses and small strains, poorly investigated in standard terrestrial geotechnics, presents a particular interest in planetary geotechnics due to reduced gravity. This is the case of the surface layer at the InSight landing site on Mars, with a gravity of $g = 3.721$ m/s^2. In this context, an experimental investigation on wave velocities at low stresses carried out on a sandy regolith simulant by using a specific novel device has been presented in a companion paper (Castillo-Betancourt et al. 2023), in which some details about the InSight mission are also provided. This paper is devoted to analysing the experimental data of this paper through a theory of contact mechanics accounting for the roughness of particles (Richart et al., 1970; Dobry et al., 1991; Bachrach et al., 2000; Bahrami et al., 2005; Butt et al., 2015). This analysis is carried out to better understand the micro-mechanisms governing wave transfers in loose sands under low stress, a domain where particle roughness plays an important role. Conclusions about the changes in Poisson ratio at low stress and strain is also derived from the analysis

2. THEORETICAL BACKGROUND

The results of Bachrach et al. (2000) are among the few available data in the domain of the in-situ investigation of the elastic behaviour of sands under low stresses and small strains. They conducted in-situ wave measurements in the Moss Landing beach (California, dry angular sand) by using a seismic line parallel to the shoreline with 20 geophones distant 30 cm and a hammer (about 50 kg) applied on a metal block as source. The Poisson ratio derived from the velocity profile between 0 and 5 m (vertical stress between 0 and 78.5 kPa with a dry unit mass of 1.7 Mg/m^3) was equal to 0.15, with no increase with depth. Bachrach et al. (2000) also presented some experimental data under lower stresses in a dense random pack of identical glass beads, and they observed that the Poisson ratio ν increased from 0.130 to 0.151 between 5 and 40 kPa.

Bachrach et al. (2000) also provided a theoretical analysis of the physics of the contacts in loose unconsolidated sands using the Hertz-Mindlin theory (HM). Mindlin (1949) provided the following expressions of the normal and shear stiffness (S_n and S_t, respectively) of two similar elastic smooth spheres in contact (see also Mavko et al., 1998):

$$S_n = \frac{4 \cdot a \cdot G_g}{1-\nu_g}, \tag{1}$$

$$S_t = \frac{8 \cdot a \cdot G_g}{2-\nu_g}, \tag{2}$$

where G_g and ν_g are the shear modulus and Poisson ratio of the sphere, respectively. a is the radius of the contact area between the spheres.

According to Hertz, a is given by:

$$a = \left[\frac{3 \cdot F \cdot R_g (1-\nu_g)}{8 \cdot G_g}\right]^{1/3}, \tag{3}$$

where R_g is the grain radius and F the compressive force between them, given by Bachrach et al., (2000) in an assembly of spheres of same radius:

$$F = \frac{4 \cdot \pi \cdot R_g^2 \cdot \sigma_3}{n(1-\phi)}, \tag{4}$$

where σ_3 is the mean stress, n is the coordination number (average number of contacts per sphere) and ϕ the porosity of the assembly.

Through statistical averaging, Digby (1981) and Walton (1987) provided the following expressions of the bulk (K_{HM}) and shear (G_{HM}) moduli of a pack of identical elastic spheres of radius R_g with mutual contact obeying the Hertz-Mindlin theory:

$$K_{HM} = \frac{n(1-\phi)}{12 \cdot \pi \cdot R_g} S_n, \tag{5}$$

$$G_{HM} = \frac{n(1-\phi)}{20 \cdot \pi \cdot R_g} (S_n + 1.5\, S_t). \tag{6}$$

The Poisson ratio of the pack can hence be expressed as follows:

$$\nu_{HM} = \frac{3K_{HM} - 2G_{HM}}{2(3K_{HM} + G_{HM})} = \frac{S_n - S_t}{4S_n + S_t} = \frac{\nu_g}{10 - 6\nu_g}. \tag{7}$$

Eq. 7 shows that the Poisson ratio of a pack of identical smooth spheres governed by the Hertz-Mindlin model (i.e., with no slippage between spheres) only depends on that of the constituent, with no dependence on the sphere radius R_g. For quartz, $\nu_g = 0.08$, yielding $\nu_{HM} = 0.0084$. This too low value indicates that, with no slippage, the radial strain of a

vertically stressed cylindrical sample is very small compared to its axial one. Such very low values are not met in sand behaviour, showing the limits of the Hertz-Mindlin approach with no slippage between particles.

2.1 Slippage between particles

By considering a zero tangential stiffness ($S_t = 0$) allowing slipping between all the grains, Bachrach et al. (2000) showed from Eq. 7 that $\nu_{HMB} = 0.25$ (where HMB stands for Hertz-Mindlin-Bachrach). This indicates that grains free to slip logically result in a larger radial expansion of a vertically stressed cylindrical sample. Bachrach et al. (2000) obtained a continuous variation of ν_{HMB} by assuming a mixture with a proportion ξ of no slipping contacts and by applying the Hashin Shtrikman bounds (Hashin and Shtrikman, 1963). From this theory, the tangential stiffness of the mixture S_t^{mix} is given by Eq. 8 and the Poisson ratio by Eq. 9. As a result, ν_{HMB} decreases from 0.25 down to 0.0084 when the fraction of no-slip contacts increases from 0 to 1, as shown in Figure 1 (with $\nu_{HMB} = 0.159$ for half grain contacts slipping - $\xi = 0.5$).

$$S_t^{mix} = S_t + \frac{1-\xi}{-\frac{1}{S_t} + \frac{2\xi(S_n+2S_t)}{5S_t(S_n+4/3S_t)}} . \tag{8}$$

$$\nu_{HMB} = \frac{S_n - S_t^{mix}}{4S_n + S_t^{mix}} . \tag{9}$$

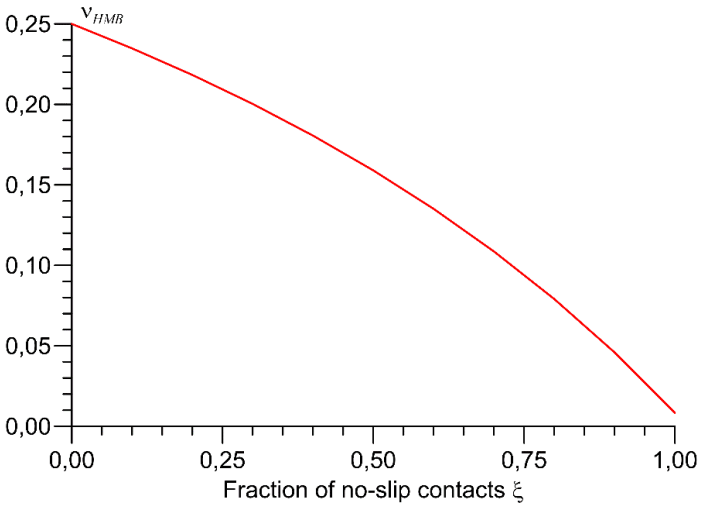

Figure 1. Change in Poisson ratio of an assembly of identical spheres with respect to the proportion of no-slip contacts ξ.

The range of magnitude of the Poisson ratio from this theory agrees well with most common measurements on sands. However, it is derived from some simplistic assumptions of perfect smooth spheres of the same radius interacting together. Rather than fully describing physical phenomena in sands (with grains of different sizes, shapes and angularity, for which ν may be larger than 0.25), it provides further insight into the macroscopic effects of some micromechanical processes. Another limitation is that ν_{HMB} (Eq. 9) is not dependent on the sphere radius R_{g} (unique in the case of identical spheres). As shown by Kumar and Madhasuda (2010), there is a dependency of ν on the grain size distribution.

2.2 Effect of particle's roughness on the elastic properties

Bachrach et al. (2000) observed that the Hertz-Mindlin theory overestimated by two the wave velocities for sands under low-stress, an issue that they relate to roughness effects at inter-particles contacts. Persson (2006) confirmed this, recalling that, for smooth contact surfaces, the Hertzian theory leads to a circular contact area $A_H = \pi a^2$ proportional to the force to a power of 2/3 (Eq. 3, $A_H \propto F^{2/3}$). Conversely, they showed that experimental data on randomly rough surfaces evidenced a contact area linearly proportional to the force ($A_H \propto F$).

According to Hertz-Mindlin's theory, compressive and shear inter-grains stiffness (S_n and S_t, respectively) are proportional with interparticle force to a power of 1/3 (Eqs. 1, 2, 3, 4). Also, from Eqs. 5, 6, and 10, the wave velocities V_{p} and V_{s} are related to the interparticle forces through the bulk (K_{HM}) and shear (G_{HM}) moduli.

$$V_P = \sqrt{\left(K_{HM} + \frac{4}{3}G_{HM}\right)/\rho_b} \text{ , and } V_S = \sqrt{\frac{G_{HM}}{\rho_b}}. \tag{10}$$

Then, assuming that force and stress are linearly related through Eq. 4, wave velocities are also related to stress, with a power of 1/6.

In contrast, in the case of rough surfaces (Persson 2006), the linear relationship between interparticle forces or stress and the contact area results in having compressive stiffnesses proportional to a power of 0.5, and wave velocities to a power of 0.25. These exponents have been mentioned by Santamarina et al. (2001), i.e., 0.25 for cone-to-plane contacts (typical of rough or angular particles) and 0.25 for spherical particles with yield at contact.

To consider the effect of roughness on sands undergoing low stresses, Bachrach et al. (2000) assume that the contact radius R_c is significantly smaller than the grain radius R_g, as shown in Figure 2.

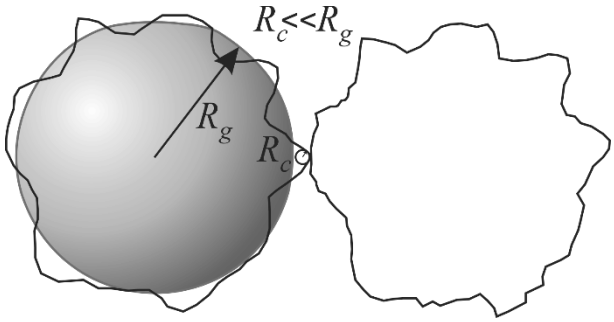

Figure 2. Schematic drawing of grains in contact with asperities, with contact radius R_c significantly smaller than R_g.

Bachrach et al. (2000) hence suggest replacing the grain radius R_g by the contact radius R_c in Eq. 3. The radius of the contact area, a_B, hence becomes:

$$\mathrm{a_B} = \left[\frac{3 \cdot F \cdot R_c (1-\nu_g)}{8 \cdot G_g}\right]^{1/3} . \tag{11}$$

Eq. 11 shows that the radius of the contact area a given by Hertz has to be corrected by a correction factor $(R_c/R_g)^{1/3}$, as follows:

$$\mathrm{a_B} = a\left(\frac{R_c}{R_g}\right)^{1/3} . \tag{12}$$

This change decreases the normal and shear stiffness S_n and S_t and the bulk and shear moduli K_{HM} and G_{HM} by a factor $(R_c/R_g)^{1/3}$ (Eqs. 5, 6), hence reducing the wave velocities V_p and V_s by a factor $(R_c/R_g)^{1/6}$ (Eq. 10).

For the Moss Landing beach sand, Bachrach et al. (2000) suggested using a constant ratio R_c/R_g=0.086. However, this value indirectly resulted from fitting in-situ measurements, without any physical link with the true particle's roughness. A more rigorous analysis is possible using theories dealing with roughness effects on bodies in contact, where contact only occurs at some discrete microcontacts points. This analysis is based on the pioneering work of Archard (1957), who demonstrated a linear proportionality between the inter-particles force and the contact area. A contact model for rough surfaces developed by

Greenwood and Williamson (1966) was used by Greenwood and Trip (1967) to provide the first theory for rough elastic spherical bodies. Majumdar and Bhushan (1991) concluded that smaller asperities are more likely to undergo small plastic deformation under increased load, and to merge together to form elastic contact points. This is in agreement with Persson (2006), who concluded that all microcontacts deform plastically, except for polished surfaces.

Most theoretical models involve complex integral equations requiring intensive iterative numerical calculations. Few analytical models dealing with rough spherical surfaces are available, except that proposed by Bahrami et al. (2005), who splitted the deformation of rough spheres under compression into two components: (i) the bulk compression of the sphere and (ii) the deformation of the asperities. In this model, asperities are described by their RMS asperity height, σ_{rms} (defined as the square root of the average of the squares of all wave heights) and the microhardness of the asperities H_{mic}. Butt et al. (2015) modified Bahrami's model by directly calculating the relationship between the contact stiffnesses of rough spheres and those obtained with the Hertz-Mindlin model for smooth spheres.

The Bahrami-Butt model assumes the following hypotheses to compute the contact behaviour between rough spheres,:

(i) The deformation mode of asperities is plastic.

(ii) The bulk deformation of the contact is elastic and occur at elastic half-space with an effective modulus of elasticity E' given by $1/E' = (1 - \nu^2)/E$. Note that the method was developed for a rigid sphere on a deformable flat surface (Figure 3). Still, the same solution is obtained for a deformable sphere on a rigid flat surface.

(iii) The pressure at microcontacts is limited by the microhardness of the softer material in contact.

(iv) Surface roughness behaves like a plastic layer in the sense that the pressure distribution can be considered as continuous pressure $P(r)$ given by the sum of pressures at all microcontacts.

(v) The microhardness is constant throughout all the contact area.

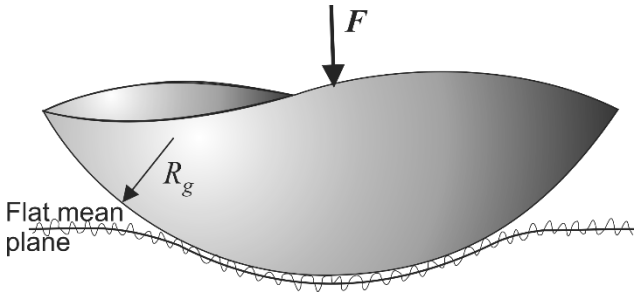

Figure 3. Schematic drawing of a sphere resting on a deformable rough surface for the Bahrami et al. (2005) model.

Bahrami-Butt's method starts by computing the Hertzian radius of the contact area given by Eq 3. Then, the method uses two non-dimensional parameters α and τ that depend on the RMS surface roughness σ_{rms} and the microhardness of the contacts H_{mic} as follows:

$$\alpha = \sigma_{\mathrm{rms}} \mathrm{R_g} / \mathrm{a}^2 \ , \tag{13}$$

$$\tau = \frac{\mathrm{E'}}{\mathrm{H_{mic}}} \left(\frac{\mathrm{R_g}}{\sigma_{\mathrm{rms}}} \right)^{1/2} . \tag{14}$$

These parameters allows computing three non-dimensional values: the non-dimensional pressure distribution P_0', the non-dimensional contact radius a_R', and the generalised pressure distribution exponent, γ, given by, respectively:

$$\mathrm{P_0'} = \frac{1}{1+1.22\alpha\tau^{-0.16}} \ , \tag{15}$$

$$\mathrm{a_R'} = 1.631 \mathrm{P_0'}^{-0.496} - 0.631 \mathrm{P_0'}^{3.358} \ , \tag{16}$$

$$\gamma = 1.5 \mathrm{P_0'} \mathrm{a_R'}^2 - 1 \ . \tag{17}$$

These non-dimensional variables allow computing the radius of the rough contact area a_R, the maximum contact stress P_0 and the stress distribution on the contact area $P(r)$ as follows:

$$\mathrm{a_R} = \mathrm{a_R'} \mathrm{a} \ , \tag{18}$$

$$\mathrm{P_0} = (1-\gamma) \frac{\mathrm{F}}{\pi (\mathrm{a_R})^2} \ , \tag{19}$$

$$\mathrm{P}(\zeta) = \gamma \mathrm{P_0} (1-\zeta^2) \ , \text{ where } \zeta = r/a_R \ . \tag{20}$$

The maximum displacement at the centre of the rough contact area, δ_R, is given by:

$$\delta_R = \frac{P_0 a_R}{E'} B(0.5, \gamma + 1) \,, \tag{21}$$

where the beta function B(0.5,γ+1) is obtained based on a function Γ, as follows:

$$B(0.5, \gamma + 1) = \frac{\Gamma(1/2)\Gamma(\gamma+1)}{\Gamma(\gamma+1.5)} \,. \tag{22}$$

The following closed type expression for function Γ was proposed by Butt et al. (2015):

$$\Gamma(x + 1) = a_1(x + a_2)^{x+a_2} \left(1 + \frac{a_3}{a_4 + x^{a_5}} + \frac{a_6}{x^{a_7} + a_8}\right) e^{-x^{a_9}} (2\pi)^{1/2} \,. \tag{23}$$

The values of the constants $a_{1..9}$ of function Γ were obtained by Butt et al. (2015) by least square parameter optimisation, leading to: a_1=0.5641886354, a_2=0.500007096, a_3=0.1091637999, a_4=1.621840565, a_5=0.992925298, a_6=0.0115834573, a_7=1.271839956, a_8=1.505508639, a_9=1. It is important to note that the purpose of Eq. 23 is to fit function Γ in a closed form rather than in its integral form; therefore, the values $a_{1..9}$ are constants, unrelated to the physics of the contact problem.

The ratio between the stiffness of the rough surface and the ideal hertzian stiffness (S_n^{Rough}/S_n^{HM}) depends on the ratio between displacements at the centre of the contact area for rough and smooth spheres δ_R/δ_H, as follows:

$$\frac{S_n^{Rough}}{S_n^{HM}} = \left(\frac{\delta_R}{\delta_H}\right)^{1/2} \,, \quad \text{with } \delta_H = a^2/R_g \,. \tag{24}$$

Finally, the Bahrami - Butt model provides the radius of the contact area of rough spheres, a_R, as follows:

$$a_R = a \frac{S_n{}^{Rough}}{S_n{}^{HM}} \,. \tag{25}$$

Note that the reduction of the contact stiffness by the ratio S_n^{Rough}/S_n^{HM} in Eq. 25 is similar to that of Bachrach et al. (2000)'s approach, in which the stiffness in Eq. 12 was reduced by the ratio $\left(\frac{R_c}{R_g}\right)^{1/3}$. However, Bachrach et al. (2000)'s approach resulted from fitting experimental results, while the Bahrami – Butt approach rests on the physics of the contact, and the relationship $\frac{S_n^{Rough}}{S_n^{HM}}$ depends on stress and the size and strength of the asperities.

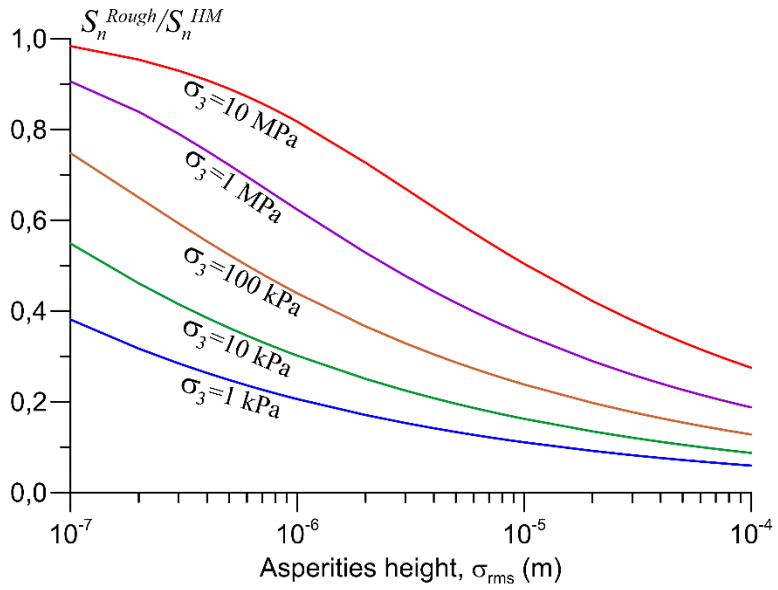

Figure 4. Ratio between the theoretical stiffness S_n^{Rough}/ S_n^{HM} of rough and smooth quartz spheres as a function of the RMS height of the asperities. The data were computed for particles with R_g=110 μm subjected to isotropic stresses σ_3 (calculated using Eq. 3 and Eq. 4, which relates force to stress) between 1 kPa to 10 MPa, and asperities microhardness H_{mic}=8.2 GPa, as suggested in Yovanovich (2006) for quartz.

Figure 4 shows the relationship $\frac{S_n^{Rough}}{S_n^{HM}}$ for different asperities height with respect to σ_{rms} at different stresses. The Figure illustrates how, when the contact stress increases, more asperities come into contact and contact stiffness increases. Unsurprisingly, the effect of roughness on stiffness is more significant at low stresses and decreases as stress increases. This is an essential conclusion for our investigation regarding wave velocities at low stresses.

The effect of particle roughness on wave velocities is obtained by introducing the reduced expression of a_R in Eqs 1…6 and then into Eq. 10, leading to the expression of V_p and V_s of an assembly of identical rough spheres. In summary, the model uses the following parameters: for the assembly: ϕ, n, ξ; for the grains, R_g, G_g, ν_g, σ_{rms}, and H_{mic}.

3. AFM ROUGHNESS ASSESSMENT OF THE FONTAINEBLEAU SAND AS A MARTIAN REGOLITH SIMULANT

To account for the rounded-subrounded shape of regolith grains on Mars (e.g. Goetz et al., 2010), we adopted in our experimental investigation (see Castillo-Betancourt et al. 2023) the NE34 Fontainebleau sand (see Delage et al. 2022a, b). It is a well-sorted silica sand (grain

density ρ_s = 2.651 Mg/m^3) from the Paris Basin with a D_{50} of 220 µm (Benahmed, 2005) to compare with the 175 µm diameter derived from thermal inertia measurements in the InSight landing site (Golombek et al., 2017, 2020). Its uniformity coefficient C_u is equal to 1.65.

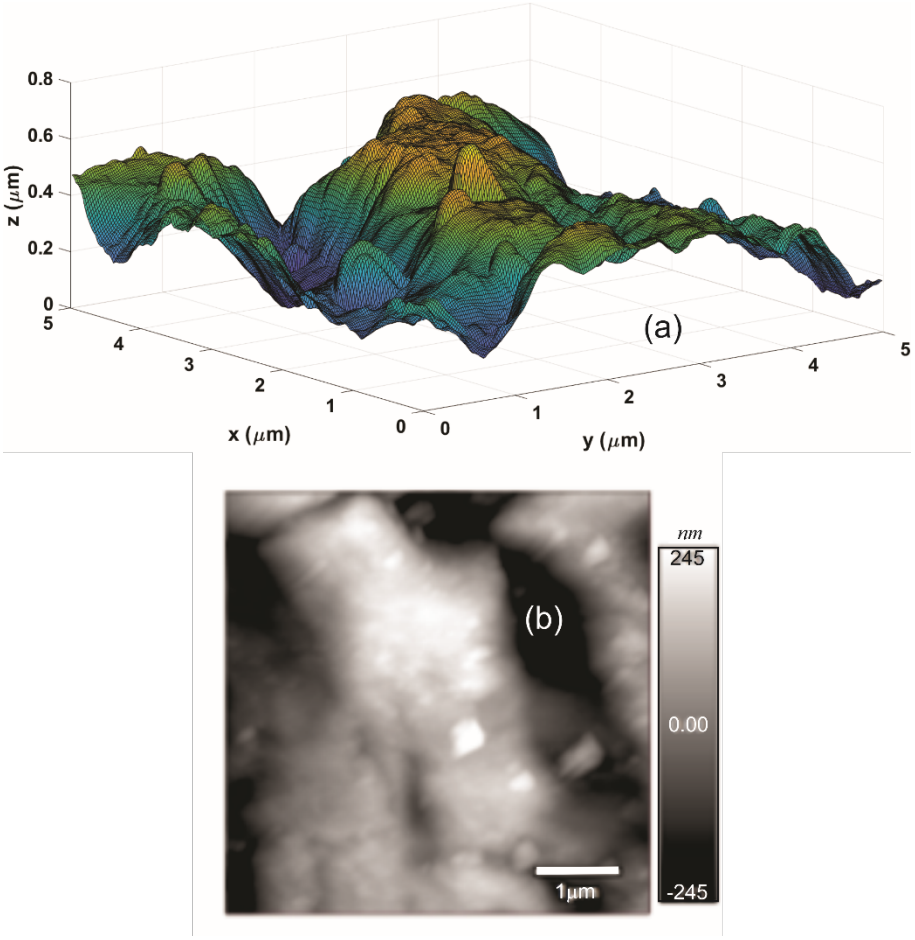

Figure 5. Grain topography measured with the AFM AC tapping mode: a) 3D image; b) Greyscale image.

Given the importance of the surface roughness at inter-grain contacts at small stresses, an investigation of the roughness of the Fontainebleau sand grains was conducted by using an Atomic Force Microscope (AFM - Cypher ES) to obtain a highly detailed surface topography using the Height Tapping Method (Binnig et al., 1986). Figure 5a displays the AFM data, with a 256 x 256 resolution in an area of 5 x 5 µm of a grain (average grain diameter is 220 µm). Compared to the (apparently) smooth grain surfaces observed in SEM, high-resolution AFM images evidence significant asperities on the surface. The greyscale image of Figure 5b shows that the rugosities height spread along in a wide span, between -245 nm (black) and + 245 nm (white). The AFM measurements give an RMS height σ_{rms} = 0.123 µm.

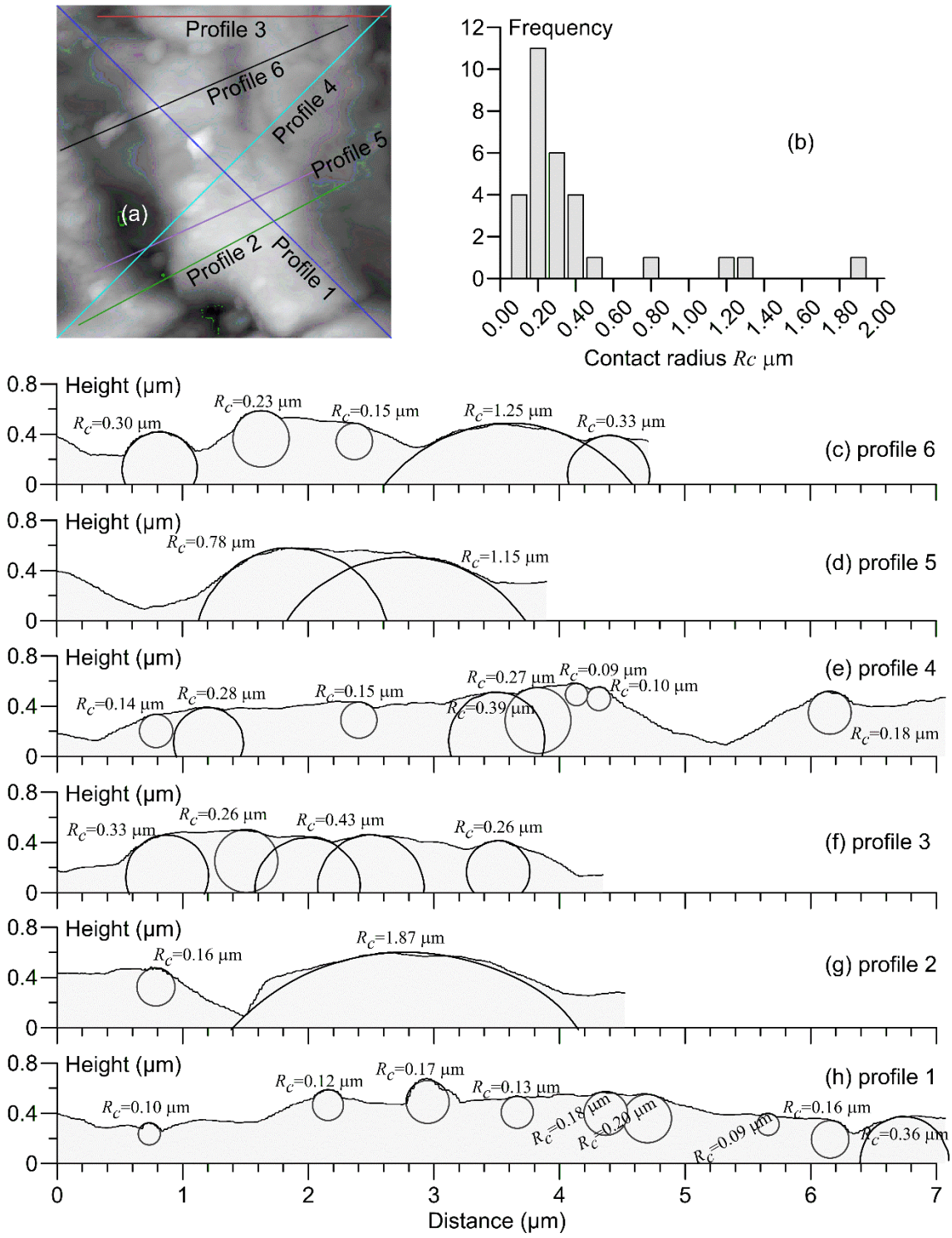

Figure 6. AFM investigation of a Fontainebleau sand grain: a) Cross profiles on the AFM measured area; b) Histogram of contact radius along the 6 profiles; c) to h) Roughness plotted along the profiles displayed in a).

The cross profiles of Figure 6c to 6h along various directions in the grey-scale image of Figure 6a provide an order of magnitude of the asperity radii. Figure 6b shows the radius histogram of the 30 circles that reasonably coincide with the asperities, providing an average radius R_c = 0.35 µm. This analysis is only a first estimate that provides approximate information about the roughness. In fact, this methodology has the following limitations:

- Only a small portion of a grain was measured with the AFM,
- Choosing 30 radios across 6 profiles does not consider the entire radius spectrum,
- The radius histogram, shown in Figure 6b, is not symmetrical and, considering that it only involves a small portion of a grain, does not include radii that have a curvature greater than the portion of the grain analyzed.
- A 2D analysis is not the most appropriate methodology to evaluate 3D asperities. It is only correct for spherical contacts. On the other hand, in the case of ellipsoidal contacts with two radii of curvature R_1 and R_2, the contact area must be evaluated using the Gaussian radius of curvature defined as $\tilde{R} = \sqrt{R_1 R_2}$, Caicedo (2018).

4. DISCUSSION

This section presents the performance of the proposed theoretical model applied to the experimental data published in the companion paper (Castillo-Betancourt 2023).

The model parameters are:

- Porosity ϕ: the average porosity of the four samples tested is $\phi = 45.5\%$.
- Coordination number n: a proper value for a loose arrangement of uniform spheres is $n = 6$ (see Mavko et al. 1989 and Caicedo 2018).
- Non-slipping fraction ξ: in sands, Bachrach et al. (2000) recommend for ξ a constant value of 0.5. However, for our experimental results, a better agreement was found with $\xi = 0.6$. This difference probably results from the different origin of the Fontainbleau sand compared to the Moss Landing beach sand.
- Grain size R_g: as in Bachrach et al. (2000)'s model, our (simplified) model considers a pack of identical spheres. The Fontainebleau sand has however a well-sorted grain size distribution with a $D_{50} = 220$µm and a uniformity coefficient $C_u = 1.65$, providing $R_g = D_{50}/2 = 110$ µm. The similarity with a pack of identical spheres is then reasonably acceptable.

- Grain's shear modulus G_g: for silica grains, $G_g = 44$ GPa (Bachrach et al., 2000).
- Grain's Poisson ratio ν_g: for silica grains, $\nu_g = 0.08$ (Bachrach et al. 2000).
- Microhardness of the asperities: H_{mic} = 8.2 GPa, according to Yovanovich (2006) for silica grains.
- Asperities height σ_{rms}: the asperities characteristics derived from the AFM data (i.e., σ_{rms} = 0.123 µm from Figure 6a and mean contact radius R_c = 0.35 µm in Figure 6b) do not result in a good agreement between our data and the model. Actually, good fitting was obtained for larger values (0.6 µm < σ_{rms} < 0.8 µm), as shown in Figure 7. This discrepancy probably comes from the imperfect evaluation of roughness that results from the 2D evaluation of only six profiles of the same grain, as described in the previous section. On the other hand, the mean value is not the most appropriate descriptor for a radius distribution shown in Figure 6b that is clearly asymmetric. Figure 7 also shows how sensitive the model is to asperities. Logically, smaller velocities are obtained for larger asperities, under the same stress.

There are various possible reasons for this discrepancy in asperities data. The first one is perhaps the approximation made between our sand and an assembly of spheres of the same diameter, like in Bachrach et al. (2000). Also, a better estimation of the asperities parameters should probably be gained from an area larger than the 5 x 5 µm one observed in our case on a single grain. However, the shape of the observed fitted curve in Figure 7 pretty well matches the data, at least above 10 kPa. For smaller stresses, the fitting is not as good, with a tendency for the points to be aligned along straight segments, exhibiting a linear change of velocities with respect to stress. This shows that something else may occur at very low stresses below 10 kPa, a trend already suspected in the experimental investigation (Castillo-Betancourt et al. 2023).

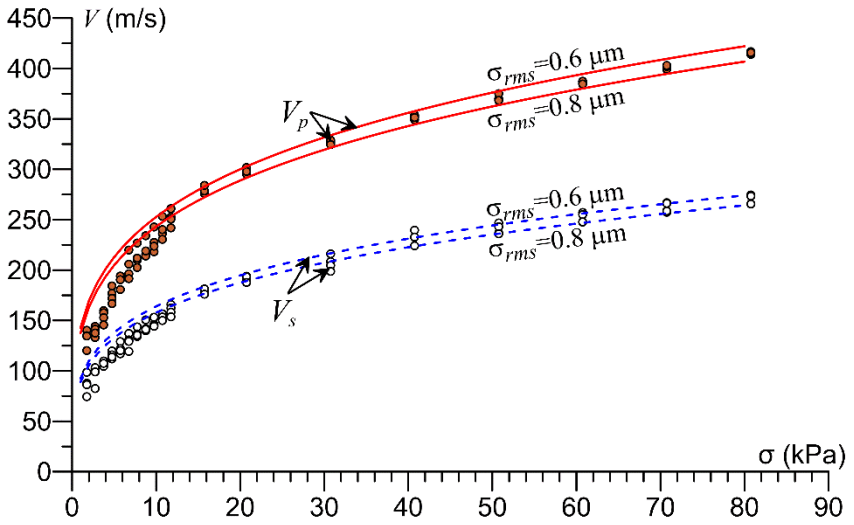

Figure 7. Comparison between measured (Castillo-Betancourt et al. 2023) and theoretical values of wave velocities.

Figure 8 shows the theoretical Poisson ratio computed from Eq. 9 for different non-slipping fractions. The Figure evidences good agreement between our experimental data and the theory for $0.55 < \xi < 0.65$. The results are close to the Poisson ratio $\nu = 0.15 \pm 0.03$ reported for rounded silica grains in Bachrach et al. (2000).

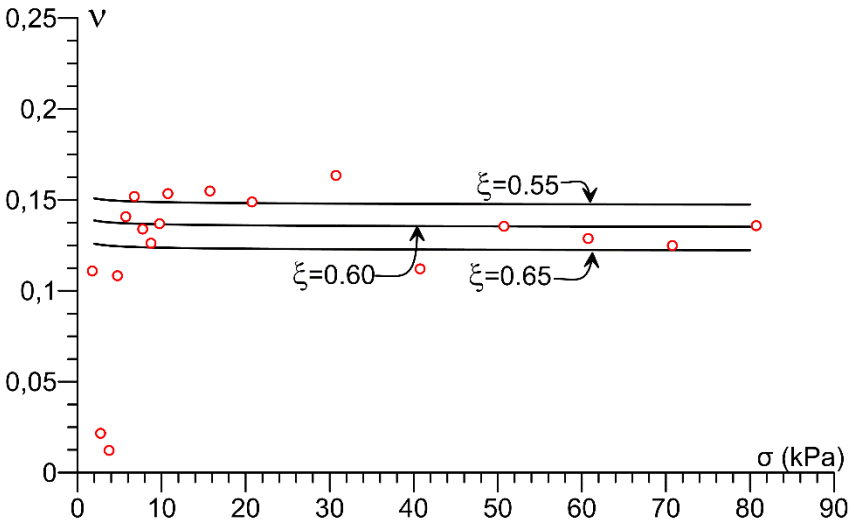

Figure 8. Comparison between measured and theoretical Poisson ratio.

Despite the good agreement of the predicted Poisson ratio, some discrepancy appears at low stresses (< 10kPa). As commented in Castillo-Betancourt et al. (2023), the larger dispersion observed below 5 kPa indicates that the performance of the experimental device is perhaps limited at very low stress, an area that certainly needs further investigation. A more accurate

device would be necessary in an area where the efficiency of standard bender elements for measuring wave velocities is perhaps limited.

Based on the (dispersed) experimental points below 5 kPa, it is not fully guaranteed that the Poisson ratio remains constant at very low stress. According to Bachrach's approach (Figure 2), a decrease in the proportion of slipping grains significantly reduces the Poisson ratio. This could be physically explained by an enhanced effect of asperities in reducing inter-grains slippage at very low stresses.

CONCLUSIONS

This paper presents a theoretical model for assessing wave velocities in loose sands subjected to low stresses. The experimental data were obtained from a companion paper (Castillo-Betancourt et al. 2023) in which a loose sample of Fontainebleau sand was used as Martian regolith simulant of the InSight landing site, and wave velocities were measured atlow stresses by using bender elements.

Based on the works of Bachrach et al. (2000), Bahrami et al. (2005) and Butt et al. (2015), a contact theory model was developed, with particular attention paid to both the proportion of inter-grains slippage occurring in a loose assembly of identical spheres, and to the effects of grains asperities, that become stronger at low stress. Bachrach et al (2000)'s approach showed that, to correctly model the elastic response of an assembly of identical spheres and to obtain a reasonable response in Poisson ratio, one has to consider some (irreversible) slippage between spheres, that are by essence not an elastic process. The values of Poisson ratio obtained in this work (and others works on sands, generally conducted at higher stresses) confirm that some slippage may occur, even in the "elastic" response of sands at very low stress (around 10^{-6} for wave transfers).

Good agreement with experimental data was obtained by the model, but we had to adopt asperities characteristics larger than those obtained by the AFM measurements carried out. This probably results from the strong assumption of assimilating our sand to an assembly of identical spheres. The AFM estimation of asperities were also carried out on a limited area (5 x 5 μm) on a single grain (average diameter 220 μm), providing an approximate determination of the asperities. The correspondence of the model with experimental data is

less satisfactory below 5 kPa, an area where the velocity change are more difficult to detect and with, perhaps, stronger effects of asperities.

The calculation of the Poisson ratio ν from wave velocities measurements confirmed the constantness of ν with stress, at least above 5 kPa. Conclusions are less clear below 5 kPa, in an area that certainly deserves more investigation. Due to possible enhanced effects of asperities and to the consequences on the proportion of sliping grains, the changes in Poisson ratio at very low stresses is to be further investigated with a more adapted device.

This study offers the possibility of assessing theoretically the elastic behaviour of sands under low stress and low strain based on the properties of the granular assembly. The proposed theory can be useful for assessing the elastic properties of other areas of Mars or the Moon. Further work being carried out by the authors includes the study of the effect of shear stresses on the mechanical response of the regolith simulant, Chaparro-López et al. (2023).

REFERENCES

Archard, J. F. (1957). Elastic deformation and the laws of friction. Proceedings of the Royal Society of London. Series A. Mathematical and physical sciences, 243(1233), 190-205.

Bachrach, R., Dvorkin, J. and Nur, A. M. (2000). Seismic velocities and Poisson's ratio of shallow unconsolidated sands. Geophysics, 65(2), 559–564. https://doi.org/10.1190/1.1444751.

Bahrami, M., Yovanovich, M. M. and Culham, J. R. (2005). A compact model for spherical rough contacts. J. Tribol. Oct 2005, 127(4): 884-889, https://doi.org/10.1115/1.2000982

Benahmed, N. (2001). Comportement mécanique d'un sable sous cisaillement monotone et cyclique : application aux phénomènes de liquéfaction et de mobilité cyclique. PhD thesis, Ecole desPonts ParisTech (in French).

Binnig, G., Quate, C. F. and Gerber, C. (1986). Atomic Force Microscope. Physical Review Letters, 56(9), 1930–1934.

Butt, S. U., Antoine, J. F. and Martin, P. (2015). Simplified stiffness model for spherical rough contacts. Tribology-Materials, Surfaces and Interfaces, 9(2), 63-70.

Caicedo, B. (2018). Geotechnics of roads: Fundamentals. CRC Press.

Castillo Betancourt, J. P., Delage, P., Caicedo B., Lognonné, P. and Banerdt B.W. (2023). Waves Velocity and Poisson Ratio in Loose Sandy Martian Regolith under Low Stresses. Part 1: Experimental Investigation. Submitted to Journal of Geophysical Research: Planets.

Chaparro-López M.J., Castillo-Betancourt J.P., Cabrera M., Caicedo B., Delage P., Lognonné P., and Banerdt B. (2023) "Dynamic Mechanical Analysis Test for Evaluating Loose Sands on a Wide Strain Range—Application to the InSight Mission on Mars," Geotechnical Testing Journal https://doi.org/10.1520/GTJ20230381.

Delage, P., Marteau, E., Vrettos, C., Golombek, M., Ansan, V., Banerdt, W. B. et al. (2022a). The mechanical properties of the Martian soil at the InSight landing site. In Proceeedings 20th International Conference on Soil Mechanics and Geotechnical Engineering, Sydney.

Delage, P., Betancourt, J. P. C., Caicedo Hormaza, B., Karakostas, F., De Laure, E., Lognonné, P. et al. (2022b). The interaction between the SEIS seismometer of the InSight Martian mission and a regolith simulant. Géotechnique, 1-12.

Digby, P. J. (1981). The effective elastic moduli of porous granular rocks. J. Appl. Mech. 48(4): 803-808.

Dobry, R., Ng, T. T., Petrakis, E., & Seridi, A. (1991). General model for contact law between two rough spheres. Journal of engineering Mechanics, 117(6), 1365-1381.

Goetz, W., Pike, W. T., Hviid, S. F., Madsen, M. B., Morris, R. V., Hecht, et al., (2010). Microscopy analysis of soils at the Phoenix landing site, Mars: Classification of soil particles and description of their optical and magnetic properties. Journal of Geophysical Research E: Planets, 115(8), 1–23. https://doi.org/10.1029/2009JE003437

Golombek, M., Kipp D., Warner I.J., Daubar I.J., Fergason R.L., Kirk R.L. et al. (2017). Selection of the InSight landing site. Space Science Review 211, 5–95.

Golombek, M., Warner, N. H., Grant, J. A., Hauber, E., Ansan, V., Weitz et al. (2020). Geology of the InSight landing site on Mars. Nature Communications, 11(1), 1–11. https://doi.org/10.1038/s41467-020-14679-1.

Greenwood, J. A. and Williamson, B. P., 1966, "Contact of Nominally Flat Surfaces," Proc. Phys. Soc., London, Sect. A, 295, pp. 300–319.

Greenwood, J. A. and Tripp, J. H., 1967, "The Elastic Contact of Rough Spheres," ASME J. Appl. Mech., 89, pp. 153–159.

Hashin, S. and Shtrikman, S., 1963, A variational approach to the elastic behavior of multiphase materials: J. Mech. Phys. Solids, 11, 127–140.

juan9715. (2023). juan9715/MRA-Bender-Element-data: Bender data public repository release (Release). Zenodo. https://doi.org/10.5281/zenodo.8161970

Kumar, J. and Madhusudhan, B. N. (2010). Effect of relative density and confining pressure on Poisson ratio from bender and extender elements tests. Géotechnique, 60(7), 561-567.

Majumdar, A. and Bhushan, B., 1991, "Fractal Model of Elastic-Plastic Contact Between Rough Surfaces," ASME J. Tribol., 113, pp. 1–11.

Mavko, G., Mukerji, T. and Dvorkin, J., 1998, The rock physics handbook: Cambridge Univ. Press.

Mindlin, R. D., 1949, Compliance of elastic bodies in contact: J. Appl. Mech., 16, 259–268.

Persson, B. N. (2006). Contact mechanics for randomly rough surfaces. Surface science reports, 61(4), 201-227.

Richart,Jr.,F.E.,Hall,J.R.,andWoods,R.D.(1970).VibrationofsoilsandfoundationsPrenticeHall,Inc.,EnglewoodCliffs,N.J.

Santamarina, J. C., Klein, K. A. and Fam, M. A. (2001). Soils and waves. New York: J. Wiley and Sons.

Walton, K. (1987). The effective elastic moduli of a random packing of spheres. Journal of the Mechanics and Physics of Solids, 35(2), 213-226.

Yovanovich, M. (2006). Micro and macro hardness measurements, correlations, and contact models. In 44th AIAA Aerospace Sciences Meeting and Exhibit (p. 979).

Acknowledgements

This work is part of the PhD thesis of Juan-Pablo Castillo Betancourt, financially supported by Universidad de los Andes (Colombia) and École des Ponts ParisTech (France). The authors are also grateful to NASA, CNES, their partner agencies and Institutions (UKSA,

SSO, DLR, JPL, IPGP-CNRS, ETHZ, IC, MPS-MPG). This paper is InSight contribution N° ICN 328.

Open Research

All the Waveform data csv files from the Bender Element measurements performed on the four samples, used for wave velocity calculations in the study and presented in the companion paper Castillo Betancourt et al. (2023) are available at the public MRA-Bender-element-repository via https://doi.org/10.5281/zenodo.8161970 . Instructions may be found on the "README" file of the repository.